Received: 20 May 2021 | Revised: 24 January 2022 | Accepted: 25 February 2022

DOI: 10.1002/asjc.2815

RESEARCH ARTICLE

WILEY

Cascade active disturbance rejection control of single-rod electrohydrostatic actuator

Xiaoxia Han[1] | **Zhixiang Chen**[2] | **Yongbao Feng**[1] | **Jian Xie**[1] | **Xiaoling Wei**[1] | **Liejiang Wei**[3]

[1]Rocket Force University of Engineering, Xi'an, China

[2]Rocket Force Sergeant Academy, Weifang, China

[3]Lanzhou University of Technology, Lanzhou, China

Correspondence
Yongbao Feng, Rocket Force University of Engineering, Hong Qing Town, Xi'an 710025, China.
Email: fyb1213@sina.com

Abstract

Electrohydrostatic actuators (EHAs) are used to replace traditional centralized hydraulic systems to reduce weight and improve efficiency and maintainability. This paper proposes a cascade active disturbance rejection control (C-ADRC) method for single-rod EHAs with parametric uncertainties and severe external disturbances. The studied EHA can be transformed into a cascade connection of a first-order pressure system and a second-order position system. Two linear active disturbance rejection controllers are designed for the inner pressure system and the outer position system to estimate and compensate for various uncertainties in the two loops, respectively. The uniqueness of the C-ADRC is that the two linear active disturbance rejection controllers are designed by making full use of the measurable states and known model information of the EHA system. It is theoretically proved that the closed-loop system is semi-globally uniformly ultimately bounded. Moreover, the proposed controller can theoretically ensure position tracking with desired accuracy as the bandwidth of extended state observers (ESOs) becomes sufficiently high. Simulation and experimental results verify the effectiveness of the proposed method.

KEYWORDS

cascade active disturbance rejection control, electrohydrostatic actuator, extended state observer, position tracking

1 | INTRODUCTION

A typical electrohydrostatic actuator (EHA) is a pump-controlled variable power transmission system. EHA systems are superior to traditional hydraulic transmissions because they afford higher power density and efficiency in addition to faster responses. EHAs have been successfully implemented in aircrafts and robots to improve the system performance [1–3]; they are now gradually being applied to large construction machinery. However, EHAs suffer from external load disturbances and internal uncertainties (e.g., parametric uncertainties, unmodeled dynamics, etc.) that affect their precision and stability.

To reduce the adverse effects of system parametric uncertainty and to improve the tracking performance of EHAs, many researchers have developed linear and nonlinear control methods for the position, velocity, and force of EHAs. The investigated strategies include variable structure sliding mode control strategies [4–11], feedback linearization methods [12, 13], backstepping controller based on Lyapunov methods [14, 15], nonlinear adaptive control methods [16, 17], robust control methods [18–20],

and active-disturbance-rejection-based methods. A nonlinear adaptive controller has negligible effect on the uncertain nonlinearity; this hinders the development of high-performance tracking controllers [21].

Active-disturbance-rejection-based methods can estimate and compensate for the total disturbance and mainly include DOBC [22], active disturbance rejection control (ADRC) [23], and uncertainty and disturbance-estimator-based control [24]. Some researchers have developed disturbance-observer-based control (DOBC) to estimate the mechanical and hydraulic disturbances of electrohydraulic systems [25, 26]. However, DOBC methods require full state information. ADRC requires minimal information regarding the system model rather than a precise mathematical model and treats the unknown dynamics and disturbances in the physical process as total disturbance, an extended state observer (ESO) is constructed to estimate the disturbances in real time, and then compensation is applied to the control signal to eliminate the effect of disturbances. Engineering applications in various industrial systems illustrate the superiority of ADRC [21, 27–34]. In recent years, studies have clarified the theoretical basis of ADRC [35]. A uniform asymptotic solution was obtained, and the exponential stability of ADRC based on singular perturbation analysis has been presented in [36]. Several modified ADRCs for nonlinear time delay systems have been studied and comprehensively compared through theoretical analysis in [37]. An innovative ADRC with control input composed of compensation has been proposed in [38], and its effectiveness has been verified through experiments with a manipulator system.

The applications of ADRC in electrohydraulic servo control systems have gradually increased. An active disturbance rejection adaptive control method was developed for motion control of hydraulic servo systems [21]. The unique features of the proposed controller were that both matched and unmatched uncertainties were estimated by two linear ESOs, and the parametric uncertainties were reduced by parameter adaptation to reduce the burden of ESOs and to avoid high gain feedback. However, this method required the full state information. In practical applications, only some states of special concern are measured in actual hydraulic servo systems, such as the position and pressure signals of the actuator. Therefore, it is necessary to further study the methods to exploit ADRC in the output feedback control of EHA systems with uncertain nonlinearities. In engineering applications, the higher order of the observer is, the more sensitive to noise will be. To overcome this limitations of high-order observers, several studies have utilized the pressure dynamics of the actuator and have proposed various cascade controllers, as in [39–43]. In [41], a sliding mode-based cascade control method with a position outer-loop and pressure inner-loop was proposed for a 6-DOF parallel robot manipulator driven by a valve-controlled asymmetric hydraulic cylinder. In [42], a four-loop nonlinear cascade controller based on an active disturbance compensation method for pump-controlled symmetrical EHA system was proposed. However, this method has many parameters to be tuned, which hinders its application in engineering.

The focus of this paper is to propose a solution that not only can make full use of the advantages of the existing control method and the known information of the EHA system but also facilitate simple parameter tuning and can therefore be practically applied in engineering. A cascade ADRC (C-ADRC) method inspired by the linear active disturbance rejection control (LADRC) and cascade control [39–41] was proposed to control a single-rod EHA. The C-ADRC comprises two cascade linear active disturbance rejection controllers (LADRC), and the uncertain disturbance of each channel can be estimated and compensated in each control channel, which effectively reduces the feedback gain. The inner-loop control gain is obtained by using the model information. The theoretical analysis shows that the overall system is semi-globally uniformly ultimately bounded. Moreover, the proposed controller can theoretically ensure the position tracking error with desired accuracy as the bandwidth of ESOs becomes sufficiently high. The simulation and experimental results show that the proposed method has excellent estimation and tracking precision, strong robustness to system uncertainty. The main contributions of this paper are summarized as follows:

1. By transforming the studied EHA system into a cascade connection of a first-order pressure system and a second-order position system, a C-ADRC method is proposed based on the model information. This method can make full use of the measurable states and known model information of the EHA system.
2. The semi-global uniform ultimate boundedness of the closed-loop is rigorous proved. It illustrates that the proposed controller can theoretically ensure desired accuracy in position tracking as the bandwidth of ESOs becomes sufficiently high. The novelty of this study lies not only in analyzing the stability of the proposed method but also in theoretically providing the parameters tuning method of the controller in engineering applications.

The remainder of this paper is organized as follows. Section 2 introduces the nonlinear mathematical model of the EHA hydraulic system. Section 3 describes the C-ADRC method and its theoretical analysis. Section 4

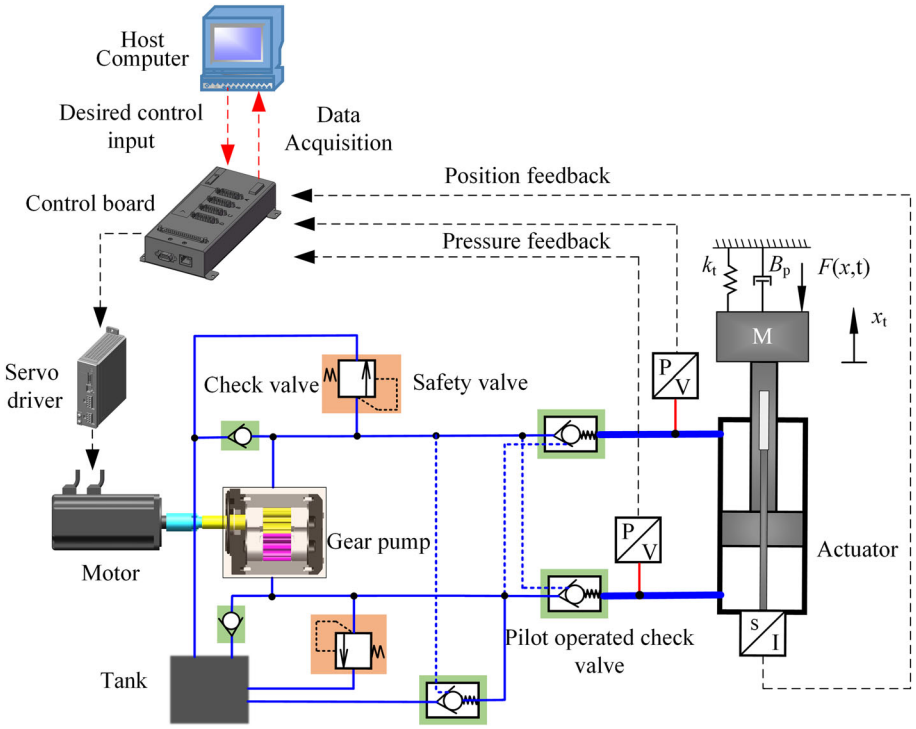

FIGURE 1 Schematic diagram of single-rod EHA system [Color figure can be viewed at wileyonlinelibrary.com]

presents the simulation results. Section 5 presents the experimental results. Finally, Section 6 presents the conclusions of this study.

2 | NONLINEAR MODEL OF EHA

Figure 1 shows a schematic diagram of a single-rod EHA system. As shown, the system mainly comprises a host computer, controller, servo driver, motor, gear pump, single-rod hydraulic cylinder, pair of hydraulic locks, and safety valve. Further, an inertial load is driven by a pump-controlled single-rod hydraulic cylinder. This study aims to overcome the spring load, viscous damping load, and disturbances $F(x,t)$ during EHA operation so that the position x_t of the load M can track a desired input trajectory as closely as possible. The dynamics equation of the EHA system can be expressed as

$$m\ddot{x}_t + F(x,t) + B_p\dot{x}_t + k_t x_t = A_1 P_1 - A_2 P_2, \qquad (1)$$

where x_t is the load displacement, m is the total mass of the load and piston, A_1 and P_1 represent the effective area and pressure of the piston-side, and A_2 and P_2 represent the effective area and pressure of the rod-side, respectively. $F(x,t) = f_f(x,t) + F_L$ represents other disturbances, such as unmodeled nonlinear frictions f_f and external load force disturbances F_L. B_p is the effective viscous damping coefficient, and k_t is the load spring stiffness. The EHA hydraulic circuit is shown in

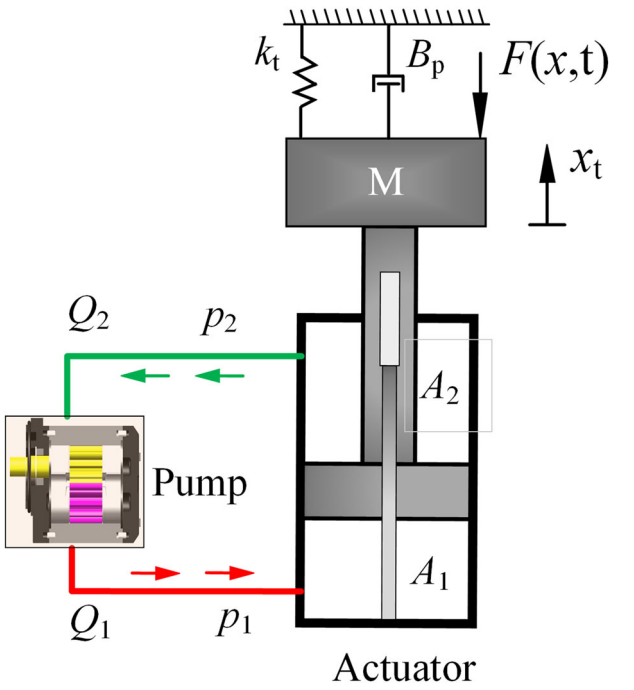

FIGURE 2 Schematic diagram of EHA hydraulic circuit [Color figure can be viewed at wileyonlinelibrary.com]

Figure 2. Considering the compressibility of hydraulic oil and the transient fluid flow dynamics, the flow continuity equations of the hydraulic cylinder can be expressed as

$$Q_1 + q_1(t) = A_1\dot{x}_t + \left(\left(V_{10} + V_{\text{pipe1}} + A_1 x_t\right)/\beta_e\right)\cdot \dot{p}_1 + C_{\text{ip}}(p_1 - p_2), \tag{2}$$

$$Q_2 + q_2(t) = A_2\dot{x}_t - \left(\left(V_{20} + V_{\text{pipe2}} - A_2 x_t\right)/\beta_e\right)\cdot \dot{p}_2 + C_{\text{ip}}(p_1 - p_2), \tag{3}$$

where Q_1 and Q_2 denote the flow rates in the actuator, β_e is the effective volume elastic modulus of the hydraulic oil, C_{ip} is the internal leakage coefficient of the hydraulic cylinder, V_{10} and V_{20} represent the initial volumes of the two chambers of the actuator, V_{pipe} is the volume of each of the two connecting pipes, and $q_1(t)$ and $q_2(t)$ represent the modeling errors in the dynamics of p_1 and p_2, respectively.

Compared with the mechanical and hydraulic subsystem, a high-response AC servo motor responds faster, with lower inertia and nonlinearity. Thus, the servo motor dynamics is neglected. Therefore, we assume the input signal u to be proportional to the pump output speed. Accordingly, Q_1 and Q_2 can be expressed as

$$Q_1 = (A_1/A_2)\,Q_2 = D_{\text{p}} k_{\text{m}}\, u, \tag{4}$$

where k_{m} is the gain with respect to the control input and D_{p} is the pump displacement.

The EHA system dynamic can be described as

$$\begin{cases} \dot{x}_t = x_v, \\ \dot{x}_v = -\dfrac{kt}{m}x_t - \dfrac{B_{\text{p}}}{m}x_v - \dfrac{F(x,t)}{m} + \dfrac{1}{m}(A_1 p_1 - A_2 p_2), \\ \dot{p}_1 = \dfrac{\beta_{\text{e}}}{V_{10} + V_{\text{pipe}} + A_1 x_t}(-A_1\dot{x}_t + Q_1 + d_1), \\ \dot{p}_2 = \dfrac{\beta_{\text{e}}}{V_{20} + V_{\text{pipe}} - A_2 x_t}(A_2\dot{x}_t - Q_2 - d_2). \end{cases} \tag{5}$$

where $d_1 = q_1(t) - c_{\text{ip}}(p_1 - p_2)$, $d_2 = q_2(t) - c_{\text{ip}}(p_1 - p_2)$, and x_v is the velocity of the piston.

The state variables are defined as $x = [x_1, x_2, x_3]^T = [x_t, \dot{x}_t, A_1 p_1 - A_2 p_2]^T$, and the state-space form equation of the EHA system can be expressed as

$$\begin{cases} \dot{x}_1 = x_2, \\ \dot{x}_2 = f_{\text{s}}(x_1) + f_{\text{d}}(x,t) + b_* x_{3\text{d}}, \\ \dot{x}_3 = -\left(\dfrac{A_1^2\beta_{\text{e}}}{V_1} + \dfrac{A_2^2\beta_{\text{e}}}{V_2}\right)\dot{x}_1 + \left(\dfrac{A_1\beta_{\text{e}}}{V_1}d_1 + \dfrac{A_2\beta_{\text{e}}}{V_2}d_2\right) \\ \quad + \left(\dfrac{A_1\beta_{\text{e}}D_{\text{p}}k_{\text{m}}}{V_1} + \dfrac{A_2}{A_1}\dfrac{A_2\beta_{\text{e}}D_{\text{p}}k_{\text{m}}}{V_2}\right)u \\ \quad = \sigma(x) + b_x u, \\ y = x_1. \end{cases} \tag{6}$$

where y is measurable output, $f_{\text{s}}(x_1) = -\frac{k_t}{m}x_1$, $f_{\text{d}}(x,t) = -(B_{\text{p}}/m)x_2 - F(x,t)/m$, $\sigma(x) = -\left(\frac{A_1^2\beta_{\text{e}}}{V_1} + \frac{A_2^2\beta_{\text{e}}}{V_2}\right)\dot{x}_1 + \left(\frac{A_1\beta_{\text{e}}}{V_1}d_1 + \frac{A_2\beta_{\text{e}}}{V_2}d_2\right)$, $V_1 = V_{10} + V_{\text{pipe1}} + A_1 x_1$, and $V_2 = V_{20} + V_{\text{pipe2}} - A_2 x_1$. $b_x = \left(\frac{A_1\beta_{\text{e}}D_{\text{p}}k_{\text{m}}}{V_1} + \frac{A_2}{A_1}\frac{A_2\beta_{\text{e}}D_{\text{p}}k_{\text{m}}}{V_2}\right)$ is used in the simulation and experiment. Further, x_1 is the position of the piston, x_2 is the velocity of the piston, and x_3 is the load force of the hydraulic cylinder.

3 | C-ADRC DESIGN

3.1 | Issues to be addressed

The hydraulic system is subjected to parametric uncertainties owing to variations in physical parameters. For designing observers and controllers, the nominal values of the physical parameters (i.e., β_{e}, B_{p}, and C_{ip}) are utilized, and the parameter deviations are lumped to the total disturbance terms, namely, $f_{\text{d}}(x,t)$ in the third line and $\sigma(x)$ in the sixth line of Equation (6). The control goal is to design the control input u to make the measurable output y track a desired input trajectory as closely as possible during the EHA operation. The observer and controller are designed under the following assumptions:

Assumption 1. The desired tracking position, velocity, and acceleration are all bounded, and p_1 and p_2 are both physically bounded by the pump outlet and inlet pressure. The functions $f_{\text{s}}(x_1)$, $f_{\text{d}}(x,t)$ and $\sigma(x)$ in Equation (6) are locally Lipschitz in a compact subset for all $x \in \mathrm{R}^3$ and all $t \in \mathrm{R}^+$.

Remark 1. In the actual EHA systems, the initial values of all states remain in a compact subset.

Assumption 2. The functions $f_{\text{d}}(x,t)$, $\sigma(x)$ and their time derivatives are all bounded for all $x \in \mathrm{R}^3$ and all $t \in \mathrm{R}^+$.

3.2 | ESO design

Based on the system model in Equation (6), we constructed two state observers under the assumption that the output displacement and the pressures, p_1 and p_2, of the actuator are measurable. $f_{\text{s}}(x_1)$ can be treated as

known dynamic variables, $f_d(x,t)$ and $\sigma(x)$ are unmatched and matched unknown uncertainty, respectively. Thus, we extended unmatched and matched uncertainty as states x_{ed1} and x_{ed2}. Let h_1 and h_2 be unknown bounded functions, the time derivatives of x_{ed1} and x_{ed2} are h_1 and h_2, respectively. Therefore, the two ESOs can be constructed as follows:

$$\begin{cases} \dot{\widehat{x}}_1 = \widehat{x}_2 + l_1(x_1 - \widehat{x}_1), \\ \dot{\widehat{x}}_2 = f_s(\widehat{x}_1) + \widehat{x}_{ed1} + b_* \widehat{x}_3 + l_2(x_1 - \widehat{x}_1), \\ \dot{\widehat{x}}_{ed1} = l_3(x_1 - \widehat{x}_1). \end{cases} \tag{7}$$

$$\begin{cases} \dot{\widehat{x}}_3 = \widehat{x}_{ed2} + b_x u + l_4(x_3 - \widehat{x}_3), \\ \dot{\widehat{x}}_{ed2} = l_5(x_3 - \widehat{x}_3). \end{cases}, \tag{8}$$

where $\widehat{x} = [\widehat{x}_1, \widehat{x}_2, \widehat{x}_{ed1}, \widehat{x}_3, \widehat{x}_{ed2}]^T \in R^5$ is the estimation of x and $l_i, i = 1,2,3,4,5$ are the observer gains. By referring to [44], let $[l_1, l_2, l_3, l_4, l_5] = [\omega_{o1}\alpha_1, \omega_{o1}^2\alpha_2, \omega_{o1}^3\alpha_3, \omega_{o2}\alpha_4, \omega_{o2}^2\alpha_5]$ with ω_{o1}, $\omega_{o2} > 0$, and ω_{o1} and ω_{o2} are the bandwidths of the two observers.

Remark 2. In this study, in contrast to the existing studies, the load force $(A_1 p_1 - A_2 p_2)$ of single-rod EHA is directly defined as a state variable to fully utilize the known model information of the EHA system and to ensure a more intuitive observer design process.

Let $\chi = [\chi_1, \chi_2, \chi_3]^T = (x - \widehat{x})/\omega_{o1}^{i-1}, j = 1,2,ed1, i = 1,2,3$, $\gamma = [\gamma_1, \gamma_2]^T = (x - \widehat{x})/\omega_{o2}^{i-1}$, and $i = 1,2.\, j = 3,\mathrm{ed}2$. Then, we have

$$\begin{cases} \dot{\chi} = \omega_{o1} A_1 \chi + B_1 \Delta_1, \\ \dot{\gamma} = \omega_{o2} A_2 \gamma + B_2 \Delta_2. \end{cases} \tag{9}$$

where $A_1 = \begin{bmatrix} -\alpha_1 & 1 & 0 \\ -\alpha_2 & 0 & 1 \\ -\alpha_3 & 0 & 0 \end{bmatrix}$, $A_2 = \begin{bmatrix} -\alpha_4 & 1 \\ -\alpha_5 & 0 \end{bmatrix}, B_1 = [0, 0, 1]^T$, $B_2 = [1, 1]^T$, $\Delta_1 = [0, \Delta f_s, h_1/\omega_{o1}^2]$, and $\Delta_2 = [0, h_2/\omega_{o2}]$.

The estimation error is defined as $\eta = [\eta_1, \eta_2, \eta_{ed1}, \eta_3, \eta_{ed2}]^T = [\chi, \gamma]^T$, then

$$\begin{cases} \dot{\eta}_1 = \left(\dot{x}_1 - \dot{\widehat{x}}_1\right)/\omega_{o1}^0 = -l_1\eta_1 + \omega_{o1}\eta_2, \\ \dot{\eta}_2 = \left(\dot{x}_2 - \dot{\widehat{x}}_2\right)/\omega_{o1}^1 = \left(-l_2\eta_1 + b_*\eta_3 + \omega_{o1}^2\eta_{ed1} + \Delta f_s\right)/\omega_{o1}, \\ \dot{\eta}_{ed1} = \left(\dot{x}_{ed1} - \dot{\widehat{x}}_{ed1}\right)/\omega_{o1}^2 = \left(-l_3\eta_1 + h_1\right)/\omega_{o1}^2. \end{cases}$$

$$\begin{cases} \dot{\eta}_3 = \left(\dot{x}_3 - \dot{\widehat{x}}_3\right)/\omega_{o2}^0 = -l_4\eta_3 + \omega_{o2}\eta_{ed2}, \\ \dot{\eta}_{ed2} = \left(\dot{x}_{ed2} - \dot{\widehat{x}}_{ed2}\right)/\omega_{o2}^1 = \left(-l_5\eta_3 + h_2\right)\omega_{o2}. \end{cases} \tag{10}$$

Let $\varepsilon = 1/\omega_{o1} = 1/\omega_{o2}$, and $0 < \varepsilon \ll 1$. Then, the dynamic of the state estimation errors can be given by

$$\varepsilon\dot{\eta} = A_\eta \eta + \varepsilon B \Delta_0, \tag{11}$$

where $A_\eta = \begin{bmatrix} A_1 & 0 \\ 0 & A_2 \end{bmatrix}, B = [B_1,\ B_2]^T$, and $\Delta_0 = [\Delta_1, \Delta_2]$..

3.3 | Controller design

The desired track state vector is defined as $r = [r_1, r_2, r_3]^T$. By combining the unknown total disturbances estimation obtained from the designed ESOs, the virtual control law x_3 is designed as

$$x_{3d} = \frac{1}{b_*}\left[k_1(r_1 - \widehat{x}_1) + k_2(r_2 - \widehat{x}_2) - \widehat{x}_{ed1} - \widehat{f}_s + r_3\right], \tag{12}$$

and the actual control input can be designed as

$$u = M\,\mathrm{sat}\left\{\frac{1}{M}\left\{\frac{1}{b_x}[k_3(x_{3d} - \widehat{x}_3) - \widehat{x}_{ed2}]\right\}\right\}. \tag{13}$$

where M is the saturation bound of the control input u. The standard saturation function is defined as $\mathrm{sat}(\vartheta) = \min\{1, |\vartheta|\}\mathrm{sign}(\vartheta)$, which is used to protect the system from peaking in the observer's transient response.

Substituting Equation (12) into Equation (13) gives

$$\begin{aligned} u = M\,\mathrm{sat}\Bigg\{ & \frac{1}{Mb_x}\Bigg\{\frac{k_3}{b_*}[k_1(r_1 - x_1 + \widehat{e}_1) \\ & + k_2(r_2 - x_2 + \widehat{e}_2)] + k_3(e_3 + e_3)\Bigg\} \\ & + \frac{1}{Mb_x}\Bigg[\frac{k_3}{b_*}\left(-\widehat{x}_{ed1} - \widehat{f}_s + r_3\right) - k_3 x_{3d} \\ & - \widehat{x}_{ed2}]\Bigg\}. \end{aligned} \tag{14}$$

where $b_x > 0$, $b_* > 0$, and $k_i > 0, i = 1,2,3$. k_i is selected as the coefficient of the Hurwitz characteristic polynomial $s^n + k_n s^{n-1} + \cdots + k_1$. For simplicity, let $s^n + k_n s^{n-1} + \cdots + k_1 = (s + \omega_c)^n$ with $\omega_c > 0$. Further, $k_i = \frac{n!}{(i-1)!(n+1-i)!}\omega_{c1}^{(n+1-i)}$, $i = 1,\ 2,$ and let $k_3 = \omega_{c2}$, where ω_{c1} and ω_{c2} are the bandwidths of the controllers of the outer and inner loops, respectively. In engineering applications, to realize a satisfactory tracking performance, ω_{c2} should be significantly greater than ω_{c1}.

The tracking error vector is defined as $e_i = r_i - x_i, i = 1,2; e_j = x_{3d} - x_3, j = 3$. Therefore, the tracking error dynamics of Equation (6) is

$$\dot{e} = A_e e + B_e \Lambda_e \eta + B_f \Delta_3. \tag{15}$$

where $A_e = \begin{bmatrix} 0 & 1 & 0 \\ -k_1 & -k_2 & 0 \\ -k_1 k_3/b_* & -k_2 k_3/b_* & -k_3 \end{bmatrix}$ is the Hurwitz matrix, $B_e = \begin{bmatrix} 0 & 0 & 0 & 0 & 0 \\ -k_1 & -k_2 & -1 & 0 & 0 \\ -k_1 k_3/b_* & -k_2 k_3/b_* & 0 & -k_3 & -1 \end{bmatrix}$,

$\Lambda_e = \begin{bmatrix} 1 & 0 & 0 & 0 & 0 \\ 0 & \omega_{o1}^1 & 0 & 0 & 0 \\ 0 & 0 & \omega_{o1}^2 & 0 & 0 \\ 0 & 0 & 0 & 1 & 0 \\ 0 & 0 & 0 & 0 & \omega_{o2}^1 \end{bmatrix}$, $B_f = [0\ 1\ 1]^T$, and

$\Delta_3 = \left[0,\ -\Delta f_s,\ \frac{k_3}{b_*}\left(\hat{x}_{ed1} + \hat{f}_s - r_3\right) + \dot{x}_{3d} + k_3 x_{3d}\right]$.

Upon combining the observer error dynamics with Equation (11), the error dynamics of the closed-loop EHA system can be expressed as

$$\dot{e} = A_e e + B_e \Lambda_e \eta + B_f \Delta_3, e(0) = e_0, \tag{16}$$

$$\varepsilon \dot{\eta} = A_\eta \eta + \varepsilon B \Delta_0, \eta(0) = \eta_0. \tag{17}$$

Remark 3. The procedure for choosing parameters of the proposed controller is provided as follows.

1. The saturation bound M in (12) is chosen such that the saturation is not activated under the state feedback.
2. For the designed ESOs in (7) and (8), a general method to choose parameters $\alpha_i, i = 1,2,3$ is $\alpha_i = \frac{(3+1)!}{(3+1-i)!i!}$, and $\alpha_i, i = 4,5$ is $\alpha_i = \frac{(2+1)!}{[(2+1-(i-3)]!(i-3)!}$. Let $\omega_{o1} = \omega_{o2}$, and $\varepsilon = 1/\omega_{o1} = 1/\omega_{o2}$ is chosen to guarantee the stability and performance requirements of the closed-loop system.
3. For the designed control law in (14), let $\omega_{c1} = \omega_{o1}/(3–5)$ and $\omega_{c2} = \omega_{o2}/(2–3)$.
4. In practice, we may need to retune the parameters ε and ω_c based on the well-tuned parameters in simulations.

3.4 | Main results

Assume that the initial states of the closed-loop system (Equations (16) and (17)) are $e_0 \in S$ and $\eta_0 \in Q$, where S and Q are both a compact set in R^3 and R^5, respectively. The closed-loop system (Equations (16) and (17)) is a standard singularly perturbed system [45]. When $\varepsilon \to 0$, the boundary layer system can be expressed as

$$\varepsilon \dot{\eta} = A_\eta \eta. \tag{18}$$

Because A_η is a Hurwitz matrix, a unique positive definite symmetric matrix $P_{\eta 1} > 0$ exists such that ${A_\eta}^T P_{\eta 1} + P_{\eta 1} A_\eta = -I$. We choose the Lyapunov function as $W(\eta) = \eta^T P_{\eta 1} \eta$. For the boundary layer system in Equation (18), the time derivative of $W(\eta)$ is

$$\dot{W}(\eta) = -\|\eta\|^2/\varepsilon \le 0. \tag{19}$$

According to the definition of Lyapunov stability, the boundary layer system in Equation (18) is asymptotically stable, $\eta \to 0$, and $t \to \infty$. Let $\eta = 0$, then the tracking error e can degenerate into

$$\dot{e} = A_e e + B_f \Delta_3. \tag{20}$$

Because A_e is a Hurwitz matrix, a unique positive definite symmetric matrix $P_{e1} > 0$ exists such that ${A_\eta}^T P_{e1} + P_{e1} A_\eta = -I$. A Lyapunov candidate function $V(e)$ is defined as $V(e) = e^T P_{e1} e$. For the degenerate system in Equation (20), the time derivative of $V(e)$ is

$$\begin{aligned} \dot{V}(e) = &-\|e\|^2 + 2e^T P_{e1} B_f \Delta_3 \le \\ &-\|e\|\left(\|e\| - 2\lambda_{\max}(P_{e1}) B_f \Delta_3\right). \end{aligned} \tag{21}$$

By referring to Assumption 1, the system dynamics $f_s(x_1)$, $f_d(x,t)$, and $\sigma(x)$ are local Lipschitz functions with respect to x. There exists $\psi > 0$ and $\phi > 1$ such that $|\Delta_3| \le (\phi - \varepsilon)\psi$. Therefore, Equation (21) can be rewritten as

$$\begin{aligned} \dot{V}(e) = &-\|e\|^2 + 2e^T P_{e1} B_f \Delta_3 \le \\ &-\|e\|(\|e\| - 2\lambda_{\max}(P_{e1})(\phi - \varepsilon)\psi). \end{aligned} \tag{22}$$

If $\|e\| \ge 2\lambda_{\max}(P_{e1})(\phi - \varepsilon)\psi$, then we have $\dot{V}(e) \le 0$. According to the definition of Lyapunov stability, the degenerate system in Equation (20) is asymptotically stable, and e and η asymptotically converge to 0 as $t \to \infty$.

Theorem 1. *If Assumptions 1–2 hold, then*

1. there exists $\varepsilon^* > 0$ such that for any $0 < \varepsilon < \varepsilon^*$, the trajectories $(e(t), \eta(t))$ of systems (16) and (17) starting from the compact set $S \times Q$ are bounded for any $t > 0$, and

2. there exists $\varepsilon_1^* = \varepsilon_1^*(\xi_1) > 0$ and $T_1 = T_1(\xi_1)$ for any $\xi_1 > 0$ such that

$$\|e(t)\| + \|\eta(t)\| \le \xi_1, \ \forall t \ge T_1, \tag{23}$$

for any $0 < \varepsilon < \varepsilon_1^*$.

Proof of Theorem 1. The proof consists of three steps. The first step is to prove the positive definite invariance of an appropriately selected set Λ that can be arbitrarily small in the direction of the error variable. The second step is to prove that any state trajectory of the closed-loop system (Equations (16) and (17)) starting from the compact set $S \times Q$ will enter the invariant set within a finite time. The third step is to prove that the state trajectory $(e(t), \eta(t))$ can approach the state origin with arbitrary precision.

Step 1: By referring to Assumption 1, for any $(e(t), \eta(t)) \in S \times Q$, the system dynamics $f_s(x_1)$, $f_d(x,t)$, and $\sigma(x)$ are local Lipschitz functions with respect to x. Combined with the continuous differentiability of the control input u, there exist $L_1, L_2, L_3, L_4 > 0$ such that

$$\|B_e \Lambda_e \eta\| \le L_1 \|\eta\|, \tag{24}$$

$$|\Delta_1| \le \varepsilon L_2 \|\eta\| \text{ and } |\Delta_2| \le L_3 + \varepsilon L_4 \|\eta\|, \tag{25}$$

Assume that $\Lambda = \{V(e) \le c\} \times \{W(\eta) \le \rho\varepsilon^2\}$, where $c \ge \lambda_{\max}(P_{e1}) \|e_0\|^2$.

Lemma 1. Assuming that there exist $\varepsilon_1 \ge 0$ and a constant ρ that depends on ε_1, the compact set Λ is positive definite invariant for any $\varepsilon \in (0, \varepsilon_1]$.

Proof. For the tracking error e of the subsystem in Equation (16), we have

$$\begin{aligned} \dot{V}(e) &= -\|e\|^2 + 2e^T P_{e1} B_e \Lambda_e \eta + 2e^T P_{e1} B_f \Delta_3 \\ &\le -\|e\|(\|e\| - 2\lambda_{\max}(P_{e1})(L_1\|\eta\| + (\phi - \varepsilon)\psi)). \end{aligned} \tag{26}$$

To make $\dot{V}(e) \le 0$ hold for any $(e(t), \eta(t)) \in \{V(e) = c\} \times \{W(\eta) \le \rho\varepsilon^2\}$,

$$\|e\| \ge 2\lambda_{\max}(P_{e1})(L_1\|\eta\| + (\phi - \varepsilon)\psi). \tag{27}$$

is necessary.

Additionally,

$$\lambda_{\min}(P_{e1})\|e\|^2 \le V(e) \le \lambda_{\max}(P_{e1})\|e\|^2, \text{and} \tag{28}$$

$$\lambda_{\min}(P_{\eta 1})\|\eta\|^2 \le W(\eta) \le \lambda_{\max}(P_{\eta 1})\|\eta\|^2. \tag{29}$$

To hold Equation (27), we obtain

$$\begin{aligned} &\sqrt{\frac{c}{\lambda_{\max}(P_{e1})}} \ge 2\lambda_{\max}(P_{e1}) \left(L_1 \sqrt{\frac{\rho\varepsilon^2}{\lambda_{\min}(P_{\eta 1})}} + (\phi - \varepsilon)\psi \right), \\ &\Rightarrow \rho \le \frac{\lambda_{\min}(P_{\eta 1})}{\varepsilon^2 L_1^2} \left[\frac{\sqrt{c/\lambda_{\max}(P_{e1})}}{2\lambda_{\max}(P_{e1})} - (\phi - \varepsilon)\psi \right]^2, \end{aligned} \tag{30}$$

From Equation (30), Equation (27) holds if

$$\rho = \frac{\lambda_{\min}(P_{\eta 1})}{\varepsilon^2 L_1^2} \left[\frac{\sqrt{c/\lambda_{\max}(P_{e1})}}{2\lambda_{\max}(P_{e1})} - (\phi - \varepsilon)\psi \right]^2. \tag{31}$$

Remark 4. From Equation (30), ρ can be appropriately large for a constant $c > 0$ when ε is very small.

For the subsystem in Equation (17), the time derivative of $W(\eta)$ is

$$\begin{aligned} \dot{W}(\eta) &= -\frac{\|\eta\|^2}{\varepsilon} + 2\eta^T P_{\eta 1}(B_1\Delta_1 + B_2\Delta_2) \\ &\le -\frac{\|\eta\|^2}{\varepsilon} + 2\varepsilon\lambda_{\max}(P_{\eta 1})(L_2 + L_4)\|\eta\|^2 \\ &\quad + 2L_3\lambda_{\max}(P_{\eta 1}) \\ &\le -\frac{\|\eta\|^2}{2\varepsilon} - \|\eta\| \left(\frac{1 - 4\varepsilon\lambda_{\max}(P_{\eta 1})(L_2 + L_4)}{2\varepsilon} \|\eta\| \right. \\ &\quad \left. - 2\lambda_{\max}(P_{\eta 1}) L_3 \right). \end{aligned} \tag{32}$$

For any $(e(t), \eta(t)) \in \{V(e) \le c\} \times \{W(\eta) = \rho\varepsilon^2\}$, if $\dot{W}(\eta) \le 0$, then we have

$$\varepsilon < 1/[4\lambda_{\max}(P_{\eta 1})(L_2 + L_4)], \tag{33}$$

$$\|\eta\| \ge \frac{4\varepsilon\lambda_{\max}(P_{\eta 1}) L_3}{1 - 4\varepsilon\lambda_{\max}(P_{\eta 1})(L_2 + L_4)}. \tag{34}$$

Based on Equations (28) and (29), Equation (34) holds if

$$\sqrt{c\lambda_{\min}(P_{\eta 1})} \geq \left(\frac{8\varepsilon\sqrt{\lambda_{\max}^3(P_{\eta 1})\lambda_{\max}^3(P_{e1})}\lambda_{\max}(P_{e1})L_1L_3}{1-4\varepsilon\lambda_{\max}(P_{\eta 1})(L_2+L_4)} + 2\sqrt{\lambda_{\max}^3(P_{e1})}(\phi-\varepsilon)\psi\right). \tag{35}$$

Assuming that $\varepsilon_2 = \frac{1}{4\lambda_{\max}(P_{\eta 1})(L_2+L_4)}$,

$$f(\varepsilon) = \frac{8\varepsilon\sqrt{\lambda_{\max}^3(P_{\eta 1})\lambda_{\max}^3(P_{e1})}\lambda_{\max}(P_{e1})L_1L_3}{1-4\varepsilon\lambda_{\max}(P_{\eta 1})(L_2+L_4)} + 2\sqrt{\lambda_{\max}^3(P_{e1})}(\phi-\varepsilon)\psi.$$

In $\varepsilon_1 \in (0,\varepsilon_2)$, $f(\varepsilon)$ increases monotonically, such that $\lim_{\varepsilon\to 0} f(\varepsilon) = 0$ and $\lim_{\varepsilon\to\varepsilon_2} f(\varepsilon_2) = \infty$. Therefore, there must exist $\varepsilon_3 \in (0,\varepsilon_2)$ such that

$$f(\varepsilon_3) = \sqrt{c\lambda_{\min}(P_{\eta 1})}. \tag{36}$$

Therefore, Equation (35) holds for any $\varepsilon \in (0,\varepsilon_3)$, that is, $\dot{W}(\eta) \leq 0$ holds. Combining Equations (31) and (36) proves Lemma 1.

Remark 5. According to Equation (36), the smaller the obtained c value, the smaller is the ε_3 value. In other words, the parameters ε of the ESO must be smaller if the output feedback control accuracy requirement is higher.

Step 2: In this case, considering $e_0 \in S, \eta_0 \notin \{W(\eta) \leq \rho\varepsilon^2\}$. Because e_0 is the interior point of S, from Equations (28) and (29), $\gamma_e = \max_{e\in\partial S, \eta\in\partial Q}\{\|e\| + L_1\|\eta\| + (\phi-\varepsilon)\psi\}$ satisfies

$$\|e(t) - e(0)\| \leq \gamma_e t \text{ and } e(t) \in S. \tag{37}$$

Thus, there is a finite time T_0 that satisfies $e(t) \in S$ for any $t \in [0, T_0]$. In $t \in [0, T_0]$, the time derivative of $W(\eta)$ is

$$\dot{W}(\eta) \leq -\|\eta\|^2/2\varepsilon \text{ and } W(0) > \rho\varepsilon^2. \tag{38}$$

Further, from Equation (29), we obtain

$$\frac{dW}{dt} \leq -\frac{1}{2\varepsilon\lambda_{\max}(P_{\eta 1})}W, \Rightarrow W(t) \leq W(0)\exp\left(-\frac{1}{2\varepsilon\lambda_{\max}(P_{\eta 1})}t\right), \tag{39}$$

Then, we can estimate the time T at which $W(t)$ enters $\{W(\eta) \leq \rho\varepsilon^2\}$ as

$$W(0)\exp\left(-\frac{1}{2\varepsilon\lambda_{\max}(P_{\eta 1})}T\right) = \rho\varepsilon^2, \Rightarrow T(\varepsilon) = 2\varepsilon\lambda_{\max}(P_{\eta 1})\ln\left(\frac{W(0)}{\rho\varepsilon^2}\right). \tag{40}$$

Based on L'Hôpital's Rule, we obtain $\lim_{\varepsilon\to 0} T(\varepsilon) = 0$. Thus, there exists $\varepsilon_4 > 0$ such that $T(\varepsilon) < T_0$ for any $\varepsilon \in (0,\varepsilon_4)$.

Upon combining steps 1 and 2 of the certification process, if we let $\varepsilon^* = \min\{\varepsilon_1, \varepsilon_4\}$, then for any $\varepsilon \in (0,\varepsilon^*)$, the trajectory $(e(t),\eta(t))$ starting from $S\times Q$ will enter the positive definite invariant set Λ within a finite time T. In other words, the trajectory $(e(t),\eta(t))$ is bounded for any $t > 0$. Thus, the first conclusion of Theorem 1 is proved.

Step 3: Construct the constant $\varphi_1 = \delta_1/(4\lambda_{\max}(P_{e1})L_1 + 1)$ that holds for any $\delta_1 > 0$.

To ensure that any η belonging to the set $\{W(\eta) \leq \rho\varepsilon^2\}$ satisfies $\|\eta\| \leq \varphi_1$, from Equation (29), we obtain

$$\sqrt{\frac{\rho\varepsilon^2}{\lambda_{\min}(P_{\eta 1})}} \leq \varphi_1, \Rightarrow \varepsilon \leq \frac{1}{\psi}\left(L_2\varphi_1 + \phi - \frac{\sqrt{c/\lambda_{\max}(P_{e1})}}{2\lambda_{\max}(P_{e1})} - \right) \triangleq \varepsilon_5. \tag{41}$$

According to step 2, let $\varepsilon_1^* = \min\{\varepsilon_1, \varepsilon_5\}$. Then, the trajectory $(e(t),\eta(t))$ starting from $S\times Q$ enters the positive definite invariant set Λ within a finite time $T(\varepsilon_1^*)$. The time derivative of V(e) is

$$\dot{V}(e) = -\|e\|^2 + 2e^T P_{e1}B_e\Lambda_e\eta + 2e^T P_{e1}B_f\Delta_3 \leq -\frac{\|e\|^2}{2} - \|e\|\left(\frac{\|e\|}{2} - 2\lambda_{\max}(P_{e1})(L_1\|\eta\| + (\phi-\varepsilon)\psi)\right). \tag{42}$$

If $e(t)$ satisfies $\|e\| \geq 4\lambda_{\max}(P_{e1})(L_1\|\eta\| + (\phi-\varepsilon)\psi)$, it can guarantee $\dot{V}(e) \leq -\|e\|^2/2$. Assuming that $\varphi_2 = 4\lambda_{\max}(P_{e1})\varepsilon L_1\varphi_1$, if $\|e(T(\varepsilon_1^*))\| \geq \varphi_2$, we can estimate the time T' at which $e(t)$ enters $\{\|e(t)\| \leq \varphi_2\}$. From Equation (28), we obtain

$$\frac{dV}{dt} \leq -\frac{1}{2\lambda_{\max}(P_{e1})}V, \Rightarrow V(t) \leq V(T(\varepsilon_1^*))\exp\left(-\frac{1}{2\lambda_{\max}(P_{e1})}(t - T(\varepsilon_1^*))\right), \tag{43}$$

and T' satisfies

$$V\left(T\left(\varepsilon_1^*\right)\right)\exp\left(-\frac{1}{2\lambda_{\max}(P_{e1})}\left(T'-T\left(\varepsilon_1^*\right)\right)\right) = \lambda_{\min}(P_{e1})\varphi_2^2, V\left(T\left(\varepsilon_1^*\right)\right) \geq \lambda_{\max}(P_{e1})\varphi_2^2. \quad (44)$$

From Equation (44), we obtain $T' = T\left(\varepsilon_1^*\right) + 2\lambda_{\max}(P_{e1})\ln\left(V\left(T\left(\varepsilon_1^*\right)\right)/\lambda_{\min}(P_{e1})\varphi_2^2\right)$. Let $T_1 = T'$. By combining Equations (41) and (44), for any $t > T_1$, we obtain

$$\|e(t)\| + \|\eta(t)\| \leq \varphi_1 + \varphi_2 = \frac{4\lambda_{\max}(P_{e1})\varepsilon L_1 + 1}{4\lambda_{\max}(P_{e1})L_1 + 1}\delta_1 \leq \delta_1. \quad (45)$$

Thus, the second conclusion of Theorem 1 is correct, Q.E.D.

Figure 3 provides a schematic diagram of the C-ADRC structure.

Remark 6. It is theoretically shown that the tracking accuracy of proposed controller is sufficiently high as the bandwidth of the ESO approaches infinity ($\varepsilon \to 0$). On the other hand, in practice, the bandwidth of ESO should be determined by considering the trade-off between the estimation performance and the limitations (e.g., noise-sensitivity, time-delay, etc.).

4 | SIMULATION RESULTS AND DISCUSSION

The mathematical models of the EHA and C-ADRC studied in this paper were established in the MATLAB/Simulink software. In the simulation, the sampling time is set as 0.001 s, and the Euler method is utilized to discretize the continuous closed-loop system. The nominal values of system parameters listed in Table 1 were used. The spring load is considered in all the simulations.

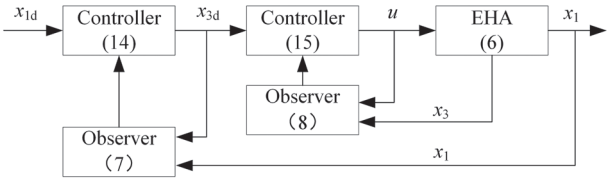

FIGURE 3 Schematic of C-ADRC structure

In addition, the performance of the proposed control method is assessed using the following three performance indices, i.e., the maximum, average, and standard deviation of the estimation and tracking errors marked as M_e, μ_{av}, and σ_s, respectively [10].

4.1 | Square-wave input tracking

The dynamic response for a square-wave input with transition process is first analyzed. The constant load force disturbance is set to 5000 N at 8 s to verify the estimation performance and control robustness, and ω_{c2} is set to be more than two times ω_{c1}. The controller parameters are given as $b_* = 0.01$, $\omega_{c1} = 20$, $\omega_{c2} = 40$, $\omega_{o1} = 100$, and $\omega_{o2} = 100$. Figure 4 and Table 2 show the estimation performance of the proposed method. It can be seen that the estimated state variables tracked the actual state variables well. The maximum estimation error of x_t is 0.13239 mm. At 8 s, a small peak appeared in the position tracking owing to external disturbances. However, it quickly returned to the set position. The maximum estimation error of the force reaches 21.9481 N when external disturbances occur. Figure 5 shows the disturbance estimates in the two channels of the C-ADRC controller. This figure shows that the proposed controller can well estimate the disturbance changes in the two control channels.

Figure 6 and Table 3 show the position tracking performance of the C-ADRC controller. They show that the proposed controller achieves good tracking performance and has excellent anti-disturbance ability. Further, Table 3 shows that the maximum tracking error of the displacement and force are 0.50969 mm and 413.2487 N, which are less than the desired value by 5.1% and 7%, respectively. As the spring load weakens the stiffness characteristic of the system, the tracking errors of displacement and load force are large at 8 s. However, when

TABLE 1 Parameters

Parameter	Value	Unit	Parameter	Value	Unit
k_t	110	$N{\cdot}mm^{-1}$	V_{10}	1×10^4	mm^3
B_p	200	N·s/m	V_{20}	7.486×10^5	mm^3
m	100	kg	V_{pipe}	1.41×10^4	mm^3
A_1	5024	mm^2	β_e	1700	MPa
A_2	2461.76	mm^2	D_p	1.25	ml/r
C_{ip}	0.26×10^{-8}	$mm^3/s/MPa$	k_m	300	/

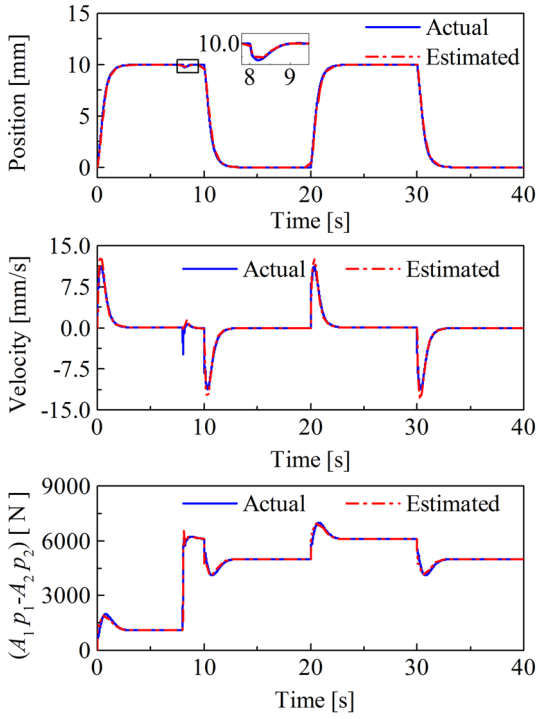

FIGURE 4 Estimation of each state variable [Color figure can be viewed at wileyonlinelibrary.com]

TABLE 2 Performance indices of state estimation

Estimation error	M_e	μ_{av}	σ_s
Position	0.13239	0.00022	0.03225
Force	21.9481	0.01668	0.9649

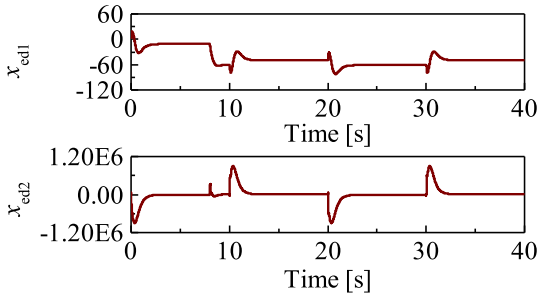

FIGURE 5 Disturbance estimation of C-ADRC controller [Color figure can be viewed at wileyonlinelibrary.com]

a large external disturbance is suddenly applied, the instantaneous high-frequency fluctuation is greatly weakened. The control input signal u increases rapidly when the position signal changes as shown in Figure 6. When an external disturbance occurs at 8 s, the control signal u is quickly compensated.

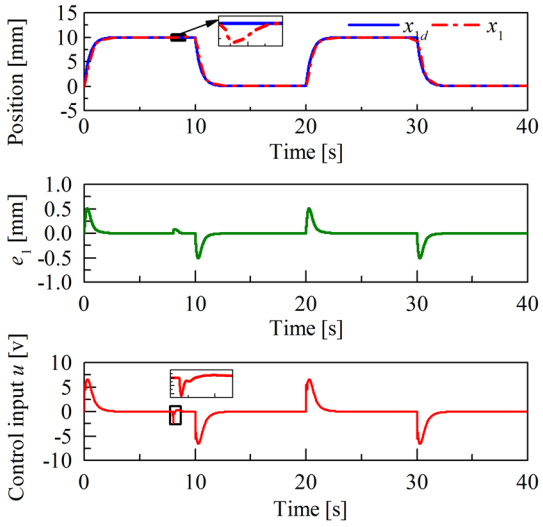

FIGURE 6 Tracking performance and control input [Color figure can be viewed at wileyonlinelibrary.com]

TABLE 3 Performance indices of state tracking

Indices	M_e	μ_{av}	σ_s
e_1	0.50969	0.00089	0.1069
e_3	413.2487	0.02321	19.59217

In Equation (6), the spring load force $f_s(x_1)$ is treated as a known disturbance, which is not included in the total disturbance x_{ed1} of the outer-loop. To analyze the impact of model uncertainty on tracking performance, $f_s(x_1)$ is classified as the total disturbance and known disturbance, respectively, and the position tracking performances are compared, as shown in Figure 7. As can be observed, when $f_s(x_1)$ is treated as a known disturbance to be compensated, the position tracking error is slightly smaller. Thus, it is necessary to use as much model information as possible in the ADRC controller design to improving the tracking accuracy.

4.2 | Sinusoidal input tracking

To verify the tracking performance of the proposed controller under sinusoidal signals, the reference position $x_{1d}(t) = 6\sin(0.2t) + 6$ is used, which ensures that x_{1d} is bounded for Assumption 1. The load force disturbance is also set to 5,000 N at 8 s. The controller parameters are given as $b_* = 0.01$, $\omega_{c1} = 15$, $\omega_{c2} = 30$, $\omega_{o1} = 60$, and $\omega_{o2} = 60$. Figure 8 and Table 4 show the estimation performance of the proposed controller. Figure 8 shows that the estimated state variables can track the actual state

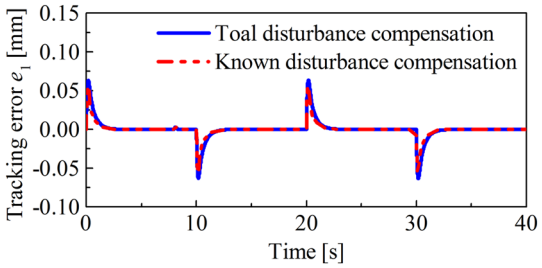

FIGURE 7 Comparison of position tracking error considering model uncertainty [Color figure can be viewed at wileyonlinelibrary.com]

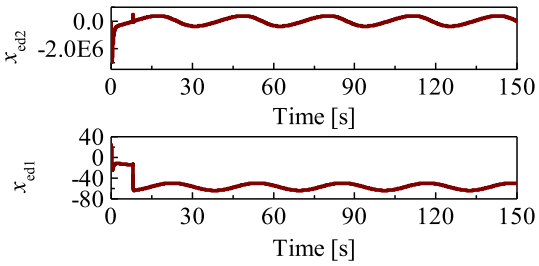

FIGURE 9 Disturbance estimation of C-ADRC controller [Color figure can be viewed at wileyonlinelibrary.com]

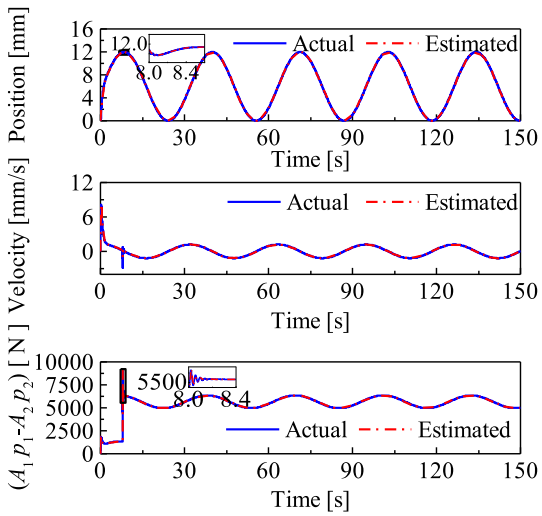

FIGURE 8 Estimation results of proposed state observer [Color figure can be viewed at wileyonlinelibrary.com]

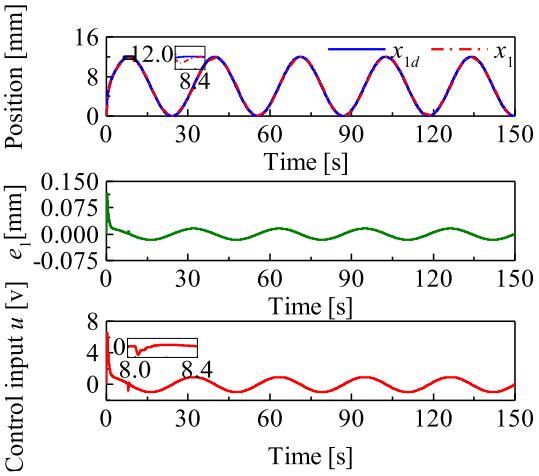

FIGURE 10 Position tracking results and control input [Color figure can be viewed at wileyonlinelibrary.com]

TABLE 4 Performance indices of state estimation

Estimation error	M_e	μ_{av}	σ_s
Position	0.00559	1.54E−6	1.32E−4
Force	575.171	0.0012	10.9258

TABLE 5 Performance indices of state tracking

Indices	M_e	μ_{av}	σ_s
e_1	0.1154	1.42E−5	0.01311
e_3	769.17	0.02097	20.0599

variables well after the disturbance occurs at 8 s. When a disturbance occurs, the actual state change can be well estimated after a certain period. Table 4 shows that the maximum estimation error of the displacement does not exceed 0.05%. Figure 9 shows the estimation of disturbances in the two channels of the C-ADRC controller. As shown, the proposed observer has excellent observation performance.

Figure 10 and Table 5 show that the proposed method has good dynamic tracking performance. When a disturbance occurs at 8 s, the displacement fluctuation is negligible, and the tracking error fluctuates but quickly becomes stable. Compared to the displacement, the system load force is more sensitive to external disturbances. As shown in Table 5, the maximum tracking error of the displacement is less than 0.12 mm. The maximum tracking error of load force at 8 s is approximately 12.6% of the given load force, which is less than the desired value by 0.5% after re-stabilization. The bottom curve of Figure 10 shows the control input signal changes with the disturbance, it indicates that the proposed controller has excellent active anti-disturbance ability.

Since the total disturbances of the EHA system are estimated and compensated, the proposed method shows excellent performance in both steady-state and dynamic tracking. The system output can also recover quickly under

a large sudden external disturbance. This further shows that the method has a strong disturbance rejection ability.

4.3 | Low-speed step input tracking

A low-speed step input with transition process is selected to validate the robustness and effectiveness of the proposed controller.

4.3.1 | Simulation A: Robustness validation

To verify the robustness of the proposed controller, the following external variable disturbance load forces based on the x_1 signal and time t are considered:

Case 1: $F_L = 2000\sin(5x_1)$,
Case 2: $F_L = 2000\sin(5x_1) \times \exp(0.1x_1)$,
Case 3: $F_L = 5000x_1 + \sin(5x_1) + \sin(20t)$,
Case 4: $F_L = x_1 + 2x_1^2 + 3x_1^3$.

Figure 11 shows the step response results under the four variable disturbance load forces. From Figure 11, the proposed method has strong anti-disturbance property against various external disturbances. Especially in Case 1, although the displacement output x_t has small oscillation at the initial stage, the fluctuation amplitude of the displacement tracking error is small. In other words, the proposed ADRC is capable of handling various disturbances.

4.3.2 | Simulation B: Effectiveness validation

To further verify the effectiveness of the proposed controller, C-ADRC proposed is compared with a cascade proportional-integral-derivative (PID) controller and a cascade backstepping controller, and the design of a backstepping controller is provided in [46]. In simulation B, the variable disturbance load force in Case 3 of simulation A is adopted. The cascade PID controller gains are $k_{po} = 2200$, $k_{io} = 1500$, $k_{do} = 0.0001$, $k_{pi} = 0.0537$, $k_{ii} = 2$, and $k_{di} = 0$, which represent the P-gain, I-gain, and D-gain of the outer-loop and inner-loop, respectively. The parameters of the backstepping controller for the outer-loop are $b = 0.01$, $c_1 = 30$, and $c_2 = 50$, and the parameter for the inner-loop is $c_3 = 125$, which represent the control gain and tuning coefficient. The tracking results and performance indices of the three compared controllers are shown in Figure 12 and Table 6. From Figure 12 and Table 6, the tracking error of PID controller is much large compared to the other

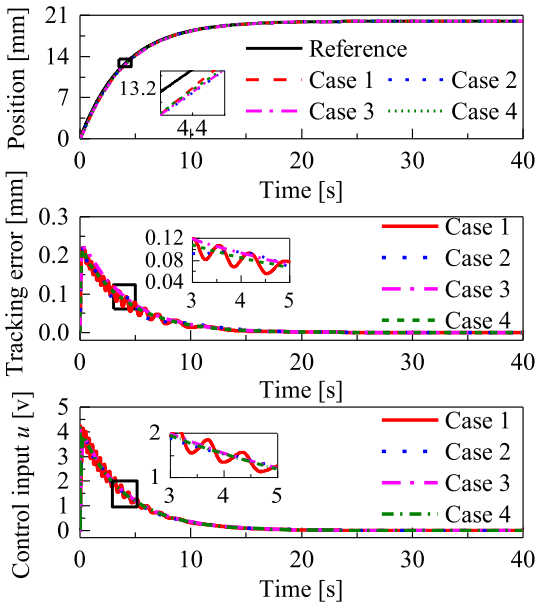

FIGURE 11 Position tracking results for various variable disturbance load forces [Color figure can be viewed at wileyonlinelibrary.com]

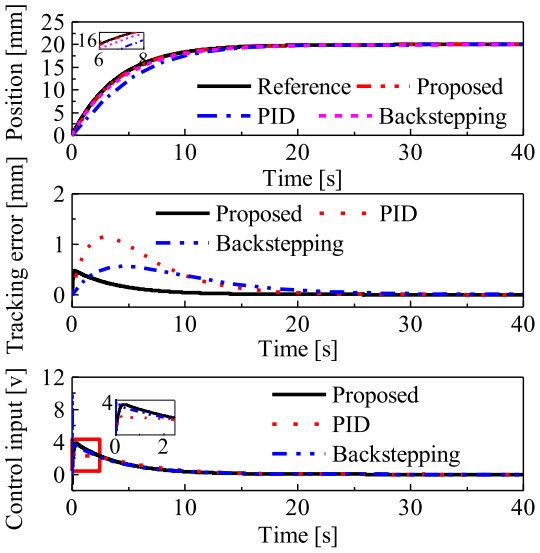

FIGURE 12 Compared tracking results [Color figure can be viewed at wileyonlinelibrary.com]

two controllers, and the control input of the proposed controller changes smoothly. Despite the maximum tracking error of the proposed method being slightly less than that in the backstepping controller, the performance indices of the proposed method are better in the overall period, as shown in Table 6. Comparing the performance of the three controllers, the proposed C-ADRC controller achieves the best tracking performance, which demonstrates the effectiveness of disturbance estimation and compensation of the proposed controller.

5 | EXPERIMENTAL VERIFICATION

The experimental platform of a single-rod EHA is shown in Figure 13. The platform consists of a spring load with $k_t = 110$ N/mm, an EHA including a single-rod hydraulic cylinder with stroke of ±75 mm, a displacement sensor to measure x_t, two pressure sensors to measure p_1 and p_2, a INOVANCE ISMH1 series AC servo motor with maximum speed of ±3000 r/min, a gear pump with displacement of 1.25 ml/r, and a measurement and control system. The measurement and control system consists of an industrial computer and the Advantech PCI data cards, with PCI-1713 AI card and PCI-1723 AO card.

TABLE 6 Tracking performance indices of the three controllers

Indices	M_e	μ_{av}	σ_s
C-ADRC	0.46946	0.04924	0.0975
PID	1.14251	0.23985	0.35573
backstepping	0.56093	0.17616	0.18973

In the experiments, the nominal values of the hydraulic system parameters are the same as those in the simulation model. The parameters of the proposed ADRC are set as $b_* = 0.01$, $\omega_{o1} = 10$, $\omega_{c1} = 1.5$, $\omega_{o2} = 10$, and $\omega_{c2} = 6$, these are obtained by real-time tuning for a given implementation. The reference position $x_{1d}(t) = 6\sin(0.02\pi t) + 6$ is used. The experimental results of the low-speed step and the sinusoidal input are shown in Figure 14 and Figure 15, respectively. Figure 14a,b shows that the proposed method is effective, and the tracking performance of the inner-loop controller can meet the requirements of the outer-loop. As shown in Figure 14c, the two ESOs can observe the disturbance in the internal and external channels in real time. From Figure 15a, the proposed controller exhibited good dynamic tracking performance. The position error in Figure 15b and the control input in Figure 15c gradually decrease. It is worth noting that the control input fluctuates greatly when the movement direction of the EHA changes.

To verify the effectiveness of the proposed C-ADRC method, a comparison is made with the cascade PID controller and the cascade backstepping controller. In the experiments, the cascade PID controller gains of outer-

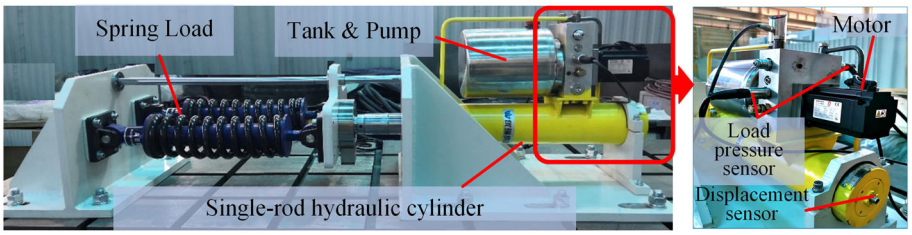

FIGURE 13 Experimental platform of EHA [Color figure can be viewed at wileyonlinelibrary.com]

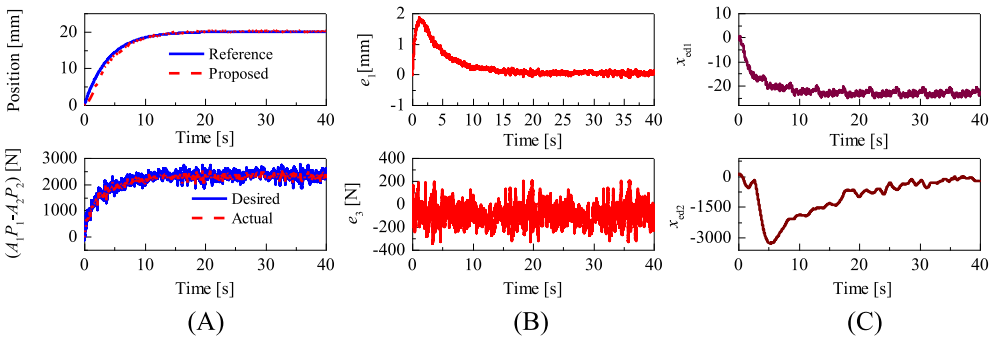

FIGURE 14 Experimental results of the low-speed step input. (A) Reference and responses. (B) Tracking errors. (C) Estimated disturbances x_{ed1} and x_{ed2} [Color figure can be viewed at wileyonlinelibrary.com]

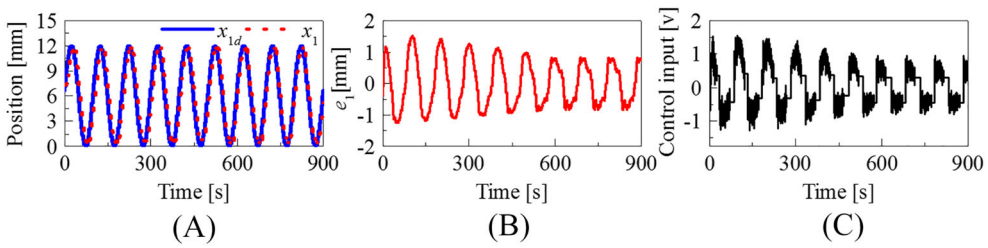

FIGURE 15 Sinusoidal input response of the proposed method. (A) Reference and responses. (B) Tracking errors. (C) Control input [Color figure can be viewed at wileyonlinelibrary.com]

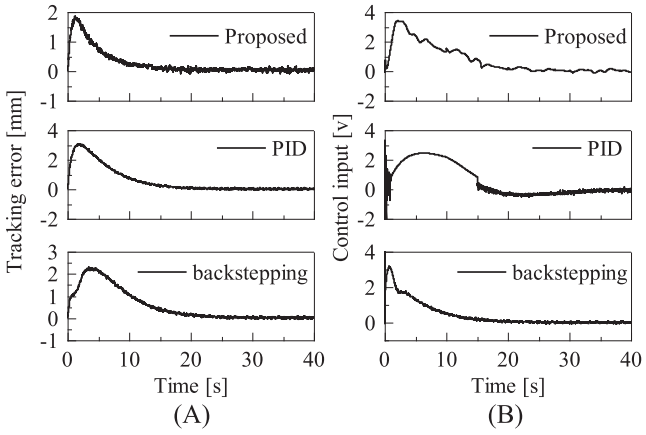

FIGURE 16 Compared tracking errors and control input. (A) Tracking errors. (B) Control input

TABLE 7 Performance indices of the state tracking

Indices	M_e	μ_{av}	σ_s
C-ADRC	1.8620	0.2654	0.4217
PID	3.0679	0.5720	0.8718
backstepping	2.2332	0.5302	0.7084

loop and inner-loop are $k_{po} = 15$, $k_{io} = 0.0001$, $k_{do} = 0.2$, $k_{pi} = 5.6$, $k_{ii} = 0.1$, and $k_{di} = 0.002$, respectively. The parameters of the backstepping controller for outer-loop are $b = 0.01$, $c_1 = 2$, and $c_2 = 5$, and the parameter for inner-loop is $c_3 = 10$. The tracking performance of the three controllers is shown in Figure 16, and the performance indices of state tracking are shown in Table 7. The experimental results show that, compared to C-ADRC, the tracking errors of the PID and backstepping controllers are more significant, especially μ_{av} and σ_s. The disturbance of the two channels can be estimated by two ESOs in C-ADRC, and the estimated disturbance can be compensated through the control input. Therefore, the proposed C-ADRC achieved the best tracking performance.

6 | CONCLUSION

In this paper, a C-ADRC method, comprising inner- and outer-loop ADRCs, was proposed to control the pressure and position of a single-rod EHA. The controller was designed to track the desired state variables, and the observers were used to estimate the state of the system using the position and pressure feedback. The results of the theoretical analysis indicate that the overall system, in the presence of various uncertainties, recovers the desired nominal performance. The simulation results show that the proposed method has strong stability and robustness to uncertainties and external disturbances of the EHA system, and the tracking performance of the outer-loop can be improved by improving the inner-loop tracking performance owing to the independence of parameter tuning. Furthermore, the comparative experimental results illustrate the effectiveness of the proposed method. In addition, the cascade design enables the parameter range of the controller to be reduced appropriately.

CONFLICT OF INTRESTEST

The authors declare that they have no known competing financial interests or personal relationships that could have appeared to influence the work reported in this paper.

AUTHOR CONTRIBUTIONS

Xiaoxia Han: Conceptualization, data curation, formal analysis, methodology, software, validation. **Zhixiang Chen:** Conceptualization, formal analysis, methodology, software. **Yongbao Feng:** Conceptualization, supervision, validation. **Jian Xie:** Project administration, resources, supervision. **Xiaoling Wei:** Software. **Liejiang Wei:** Validation.

ORCID

Xiaoxia Han https://orcid.org/0000-0002-2880-0419

REFERENCES

1. S. R. Habibi and G. Singh, *Derivation of design requirements for optimization of a high performance hydrostatic actuation system*, Int J Fluid Power **1** (2000), no. 2, 11–27. https://doi.org/10.1080/14399776.2000.10781088
2. J. Yao, P. Wang, Z. Dong, D. Jiang, and T. Sha, *A novel architecture of electro-hydrostatic actuator with digital distribution*, Chin. J. Aeronaut. **34** (2021), no. 5, 224–238. https://doi.org/10.1016/j.cja.2020.08.012
3. W. Kim and D. Won, *Nonlinear position control with nonlinear coordinate transformation using only position measurement for single-rod electro-hydrostatic actuator*, Mathematics **8** (2020), no. 8, 1273. https://doi.org/10.3390/math8081273
4. H. X. Zhuang, Q. L. Sun, and Z. Q. Chen, *Sliding mode control for electro-hydraulic proportional directional valve-controlled position tracking system based on an extended state observer*, Asian J Control **23** (2021), no. 4, 1855–1869. https://doi.org/10.1002/asjc.2432
5. M. Jerouane & F. Lamnabhi-Lagarrigue A new sliding mode controller for a hydraulic actuators, In Proceedings of the 2001 Conference on Decision and Control, 1(2001), 908–913.
6. H.-M. Chen, J.-C. Renn, and J.-P. Su, *Sliding mode control with varying boundary layers for an electro-hydraulic position servo system*, Int. J. Adv. Manuf. Technol. **26** (2005), no. 1, 117–123. https://doi.org/10.1007/s00170-004-2145-0
7. M. Wang, Y. Wang, R. Yang, Y. Fu, and D. Zhu, *A sliding mode control strategy for an electrohydrostatic actuator with damping*

variable sliding surface, Actuators **10** (2020), no. 1, 3. https://doi.org/10.3390/act10010003
8. C. Guan and S. Pan, *Adaptive sliding mode control of electro-hydraulic system with nonlinear unknown parameters*, Control Eng Practice **16** (2008), no. 11, 1275–1284. https://doi.org/10.1016/j.conengprac.2008.02.002
9. Y. Lin, Y. Shi, and R. Burton, *Modeling and robust discrete-time sliding mode control design for a fluid power electro-hydraulic actuator (EHA) system*, IEEE/ASME Trans Mechatron **18** (2011), no. 1, 1–10. https://doi.org/10.1109/TMECH.2011.2160959
10. J. Yao, Z. Jiao, and D. Ma, *Extended-state-observer-based output feedback nonlinear robust control of hydraulic systems with backstepping*, IEEE Trans Industr Electron **61** (2014), no. 11, 6285–6293. https://doi.org/10.1109/TIE.2014.2304912
11. S. H. Cho and R. Burton, *Position control of high performance hydrostatic actuation system using a simple adaptive control (SAC) method*, Mec. Dent. **21** (2011), no. 1, 109–115. https://doi.org/10.1016/j.mechatronics.2010.09.003
12. H. A. Mintsa, R. Venugopal, J.-P. Kenne, and C. Belleau, *Feedback linearization-based position control of an electrohydraulic servo system with supply pressure uncertainty*, IEEE Trans Control Syst Technol **20** (2011), no. 4, 1092–1099. https://doi.org/10.1109/TCST.2011.2158101
13. J.-H. Kwon, T.-H. Kim, J.-S. Jang, and I.-S. Lee, Feedback linearization control of a hydraulic servo system, In 2006 SICE-ICASE International Joint Conference, (2006), 455–460.
14. C. Kaddissi, J. Kenne, and M. Saad, *Identification and real-time control of an electrohydraulic servo system based on nonlinear backstepping*, IEEE/ASME Trans Mechatron **12** (2007), no. 1, 12–22. https://doi.org/10.1109/TMECH.2006.886190
15. L. Tian, L. Qian, and L. Chen, Sliding mode control based on backstepping method for electro-hydraulic single-rod actuator, In 2015 IEEE International Conference on Information and Automation, (2015) 2326–2329.
16. J. Yao, W. Deng, and Z. Jiao, *Adaptive control of hydraulic actuators with LuGre model based friction compensation*, IEEE Trans Industr Electron **62** (2015), no. 10, 6469–6477. https://doi.org/10.1109/TIE.2015.2423660
17. C. Kaddissi, J.-P. Kenne, and M. Saad, *Indirect adaptive control of an electrohydraulic servo system based on backstepping*, IEEE/ASME Trans Mechatron **16** (2010), no. 6, 1171–1177. https://doi.org/10.1109/TMECH.2010.2092785
18. X. J. Chen, D. Li, X. B. Yang, and Y. C. Yu, *Identification recurrent type 2 fuzzy wavelet neural network and L2-gain adaptive variable sliding mode robust control of electro-hydraulic servo system (EHSS)*, Asian J Control **20** (2018), no. 4, 1408–1490. https://doi.org/10.1002/asjc.1643
19. C. Guan and S. Pan, *Nonlinear adaptive robust control of single-rod electro-hydraulic actuator with unknown nonlinear parameters*, IEEE Trans Control Syst Technol **16** (2008), no. 3, 434–445. https://doi.org/10.1109/TCST.2007.908195
20. F. Bu and B. Yao, Desired compensation adaptive robust control of single-rod electro-hydraulic actuator, In Proceedings of the 2001 American Control Conference, 5(2001), 3926–3931.
21. J. Yao and W. Deng, *Active disturbance rejection adaptive control of hydraulic servo systems*, IEEE Trans Industr Electron **64** (2017), no. 10, 8023–8032. https://doi.org/10.1109/TIE.2017.2694382
22. W. Chen, J. Yang, L. Guo, and S. Li, *Disturbance-observer-based control and related methods: An overview*, IEEE Trans Industr Electron **63** (2015), no. 2, 1083–1095. https://doi.org/10.1109/TIE.2015.2478397
23. J. Han, *From PID to active disturbance rejection control*, IEEE Trans Industr Electron **56** (2009), no. 3, 900–906. https://doi.org/10.1109/TIE.2008.2011621
24. B. Ren, Q. Zhong, and J. Chen, *Robust control for a class of non-affine nonlinear systems based on the uncertainty and disturbance estimator*, IEEE Trans Industr Electron **62** (2015), no. 9, 5881–5888. https://doi.org/10.1109/TIE.2015.2421884
25. K. Wonhee, W. Daehee, S. Donghoon, and C. Chung, *Disturbance observer-based position tracking controller in the presence of biased sinusoidal disturbance for electrohydraulic actuators*, IEEE Trans Control Syst Technol **21** (2013), no. 6, 2290–2298. https://doi.org/10.1109/TCST.2013.2237909
26. W. Daehee, K. Wonhee, S. Donghoon, and C. Chung, *High-gain disturbance observer-based backstepping control with output tracking error constraint for electro-hydraulic systems*, IEEE Trans Control Syst Technol **23** (2014), no. 2, 787–795. https://doi.org/10.1109/TCST.2014.2325895
27. W. Xue, W. Bai, S. Yang, K. Song, Y. Huang, and H. Xie, *ADRC with adaptive extended state observer and its application to air–fuel ratio control in gasoline engines*, IEEE Trans Industr Electron **62** (2015), no. 9, 5847–5857. https://doi.org/10.1109/TIE.2015.2435004
28. W. Wei, W. Xue, and D. Li, *On disturbance rejection in magnetic levitation*, Control Eng Practice **82** (2019), 24–35. https://doi.org/10.1016/j.conengprac.2018.09.018
29. F. Beltran-Carbajal, A. Favela-Contreras, A. Valderrabano-Gonzalez, and J. C. Rosas-Caro, *Active disturbance rejection control of a magnetic suspension system*, Asian J Control **17** (2015), no. 3, 842–854. https://doi.org/10.1002/asjc.934
30. L. Sun, D. Li, K. Hu, K. Lee, and F. Pan, *On tuning and practical implementation of active disturbance rejection controller: A case study from a regenerative heater in a 1000 MW power plant*, Industr Eng Chem Res **55** (2016), no. 23, 6686–6695. https://doi.org/10.1021/acs.iecr.6b01249
31. L. Qu, W. Qiao, and L. Qu, *An extended-state-observer-based sliding-mode speed control for permanent-magnet synchronous motors*, IEEE J Emerg Sel Topics Power Electron **9** (2020) no. 2, 1605–1613. https://doi.org/10.1109/TPEL.2020.3003666
32. Q. Zheng, H. Richter, and Z. Gao, *Active disturbance rejection control for piezoelectric beam*, Asian J Control **16** (2014), no. 6, 1612–1622. https://doi.org/10.1002/asjc.854
33. S. Zhao and Z. Gao, *An active disturbance rejection based approach to vibration suppression in two-inertia system*, Asian J Control **15** (2013), no. 2, 350–362. https://doi.org/10.1002/asjc.552
34. Y. Wang, W. Zhang, H. Dong, and L. Yu, *A LADRC based fuzzy PID approach to contour error control of networked motion control system with time-varying delays*, Asian J Control **22** (2020), no. 5, 1973–1985. https://doi.org/10.1002/asjc.2080
35. Q. Zheng and Z. Gao, *Active disturbance rejection control: Some recent experimental and industrial case studies*, Control Theory Technol **16** (2018), no. 4, 301–313. https://doi.org/10.1007/s11768-018-8142-x
36. S. Shao and Z. Gao, *On the conditions of exponential stability in active disturbance rejection control based on singular*

perturbation analysis, Int J Control **90** (2017), no. 10, 2085–2097. https://doi.org/10.1080/00207179.2016.1236217

37. S. Chen, W. Xue, S. Zhong, and Y. Huang, *On comparison of modified ADRCs for nonlinear uncertain systems with time delay*, Sci China Inf Sci **61** (2018), no. 7, 070223, 1–15. https://doi.org/10.1007/s11432-017-9403-x
38. S. Chen and Z. Chen, *On active disturbance rejection control for a class of uncertain systems with measurement uncertainty*, IEEE Trans Industr Electron **68** (2020), no. 2, 1475–1485. https://doi.org/10.1109/TIE.2020.2970623
39. M. Li, W. Shi, J. Wei, J. Fang, K. Guo, and Q. Zhang, *Parallel velocity control of an electro-hydraulic actuator with dual disturbance observers*, IEEE Access **7** (2019), 56631–56641. https://doi.org/10.1109/ACCESS.2018.2886583
40. A. Li, D. Meng, B. Lu, and Q. Yang, *Nonlinear cascade control of single-rod pneumatic actuator based on an extended disturbance observer*, J Central South Univ **26** (2019), no. 6, 1637–1648. https://doi.org/10.1007/s11771-019-4118-3
41. H. Guo, Y. Liu, G. Liu, and H. Li, *Cascade control of a hydraulically driven 6-DOF parallel robot manipulator based on a sliding mode*, Control Eng Practice **16** (2008) no. 9, 1055–1068. https://doi.org/10.1016/j.conengprac.2007.11.005
42. M. Wang, Y. Wang, Y. Fu, R. Yang, J. Zhao, and J. Fu, *Experimental investigation of an electro-hydrostatic actuator based on the novel active compensation method*, IEEE Access **8** (2020), 170635–170649.
43. Y. Li, L. Feng, and Y. Wang, *A cascade control approach to active suspensionusing pneumatic actuators*, Asian J Control **21** (2019) no. 1, 70–88. https://doi.org/10.1002/asjc.2028
44. Q. Zheng, L. Gao, and Z. Gao, On stability analysis of active disturbance rejection control for nonlinear time-varying plants with unknown dynamics, 46th IEEE Conference on Decision and Control, (2007), 3501–3506.
45. P. Kokotovic, H. K. Khalil, and J. O. Reilly, *Singular perturbation methods in control analysis and design*, Academic Press, London, 1986.
46. Y. Li, P. Zhang, D. Li, Y. Li, and L. Yang, Backstepping adaptive control of dual-variable electro-hydraulic actuator with displacement-pressure regulation pump, 12th IEEE Conference on Industrial Electronics and Applications (ICIEA), (2017) 1206–1211.

AUTHOR BIOGRAPHIES

Xiaoxia Han received the BS degree in measurement and control technology and instruments and MS degree in mechanical and electronic engineering from the Lanzhou University of Technology, Lanzhou, China, in 2013 and 2016, respectively. She is currently pursuing the PhD degree in Rocket Force University of Engineering, Xi'an, China. Her research interests focus on control methods and thermal–hydraulic analysis of electro-hydraulic system.

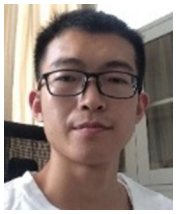

Zhixiang Chen received the BS, MS, and PhD degrees in mechanical engineering from Rocket Force University of Engineering, Xi'an, China. He is currently a lecturer with Department of Missile Launching and Power, Rocket Force Sergeant Academy, Weifang, China. His research interest includes the theoretical analysis and applications of the active disturbance rejection control.

Yongbao Feng received his MS and PhD degrees from Xi'an Research Institute of High Technology, Xi'an, China, in 2003 and 2012, respectively. He is currently a Professor with Rocket Force University of Engineering, Xi'an, China. His research areas of interest include hydraulic testing technology, intelligent hydraulic components, and electro-hydraulic control technology.

Jian Xie received his MS and PhD degrees from Xi'an Research Institute of High Technology, Xi'an, China, in 1997 and 2001, respectively. He is currently a Professor with the Rocket Force University of Engineering, Xi'an, China. His research areas of interest include high precision servo control, sliding mode control theory, automatic detection, and control of large hydraulic equipment.

Xiaoling Wei received her BS degree in measurement and control technology and instruments in 2012 and her MS degree in mechanical and electronic engineering in 2015 from the Lanzhou University of Technology, Lanzhou, China. She is currently pursuing her PhD at the Rocket Force University of Engineering, Xi'an, China. Her research interests include the design, simulation and test of hydraulic components.

Liejiang Wei received his MS degree in control theory and control engineering from Gansu University of Technology, China, in 2001, and the PhD degree in fluid mechanics from the Lanzhou University of Technology, Lanzhou, China, in

2009. He works as a full-time Professor at the Lanzhou University of Technology. His research areas of interest include electro-hydraulic control system, micro-flow/micro-pressure measurement methods, fluid mechanical testing, fluid control devices, and systems.

How to cite this article: X. Han, Z. Chen, Y. Feng, J. Xie, X. Wei, and L. Wei, *Cascade active disturbance rejection control of single-rod electrohydrostatic actuator*, Asian J Control (2022), 1–17. https://doi.org/10.1002/asjc.2815